Relative Permeability of Near-Miscible Fluids in Compositional Simulators

Alzayer, Ala N.; Voskov, Denis V.; Tchelepi, Hamdi A.

Important note
To cite this publication, please use the final published version (if applicable).
Please check the document version above.

Relative Permeability of Near-Miscible Fluids in Compositional Simulators

**Ala N. Alzayer · Denis V. Voskov ·
Hamdi A. Tchelepi**

Abstract Miscible gas injection is one of the most effective Enhanced Oil Recovery (EOR) techniques. There are several challenges in accurately modeling this process that mostly occur in the near-miscible region. The adjustment of relative permeability for near-miscible processes is the main focus of this work. The dependence of relative permeability on phase identification can lead to significant complications while simulating near-miscible displacements. We present an analysis of how existing methods incorporate compositional dependence in relative permeability functions. The sensitivity of the different methods to the choice of reference points is presented with possible guidelines to limit the modification of the relative permeabilities to physically reasonable values.

We distinguish between the objectives of reflecting near miscible behavior and ensuring smooth transitions across phase changes in the existing methods. We highlight an important link that combines the two objectives in a more general framework. We make use of Gibbs free energy as a compositional indicator to honor the generalized framework. The new approach was implemented in the Automatic Differentiation General Purpose Research Simulator (ADG-PRS) and tested on a set of near-miscible gas injection problems. We show that including compositional dependencies in the relative permeability near the critical point impacts the simulation results with significant improvements in nonlinear convergence.

F. Author
first address
Tel.: +123-45-678910
Fax: +123-45-678910
E-mail: fauthor@example.com

S. Author
second address

1 Introduction

Gas injection is among the most widely used Enhanced Oil Recovery (EOR) processes [1]. Complex nonlinear interactions take place when a gas mixture is injected into a porous medium containing oil. Components in the injected 'gas'-phase dissolve in the resident 'oil' phase, and components in the oil transfer to the gas until local chemical equilibrium is established [2]. These interactions give rise to interesting phase behaviors that can lead to fully miscible displacements. In numerical simulation of gas-injection processes, it is important to account for the compositional dependence of the relative-permeability relations in order to model the flow and transport dynamics accurately.

Darcy-based modeling of multiphase flow is based on the use of relative-permeability functions (k_r). The relative-permeability of a fluid phase describes the relation between the 'local' saturation and the flowing fraction. The k_r relations are usually written as a function of saturation only. In essence, the k_r functions lump the effects of complex rock-fluids interactions in the pore space into a saturation-only dependency. Thus, one cannot expect the saturation alone to capture the complex paths and interactions that the fluids experience. Our focus here is on the effects of interfacial tension (IFT) on the relative-permeability. Two fluid phases with zero IFT between them form a fully miscible mixture, which will flow as a single phase without trapping. Hence, the relative-permeability curves are expected to become linear as the IFT approaches zero with zero residual saturations and end-points of unity (Figure 1).
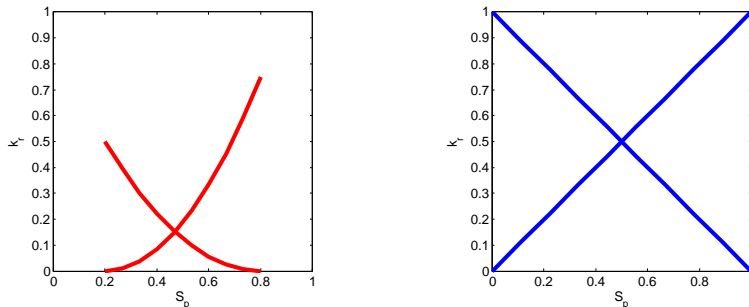

Fig. 1 *An example of an immiscible (left) and miscible (right) relative permeability curve.*

As pointed out by [3] and [4], there is no consensus on how the relative-permeability curves change as miscibility is approached. Experimental investigations of miscibility development is a rich topic and will not be covered in this paper. Instead, our focus here is capturing the compositional dependence of the k_r relations and to study the impact on the computed predictions of gas-injection EOR processes.

2 Compositional Dependence of Relative Permeability

The methods used to capture compositional dependence of relative-permeability include: (1) reflecting miscible behavior as critical conditions are approached; (2) ensuring compositional consistency as the phase behavior evolves toward miscibility. Some methods attempt to incorporate both strategies. The two approaches are described in detail below.

2.1 Reflecting Miscibility

The main objective of these methods is to use a more representative relative-permeability curve (closer to the 45° diagonals) as miscibility is developed. The general idea is to use an interpolation parameter (F_k) to modify the relative permeability between the two ends of the spectrum (miscible vs. immiscible). The interpolation usually takes the form:

$$k_{rp}^{Cor} = F_k \cdot k_{rp}^{Imm}(S_p) + [1 - F_k] \cdot k_{rp}^{Mis}(S_p) \tag{1}$$

Figure 1 is an example of the immiscible (k_{rp}^{Imm}) and miscible (k_{rp}^{Mis}) curves. The interpolation parameter (F_k) varies from zero at complete miscibility to unity for the immiscible displacement. Details on what to consider when inter- polating between the two limits are presented by [3] and [5]. The interpolation parameter (F_k) can be written as a function of surface tension [6] in Equation 2, or the capillary number [7] in Equation 3. [7] highlight the importance of using a capillary-number dependence near the wellbore, where high velocities play a significant role, as well as the possibility of having a different indepen- dent variable for k_{rp}^{Imm} and k_{rp}^{Mis}, such as (k_{rg}/k_{ro}) instead of S_p in the case of gas-condensate wells.

$$F_k = min\left[1, \left(\frac{\sigma}{\sigma_0}\right)^n\right] \tag{2}$$

$$F_k = \frac{1}{1 + (\alpha \cdot N_{cap})^n}, \quad where \quad N_{cap} = \frac{u\mu}{\sigma} \tag{3}$$

Surface tension is usually computed in reservoir simulators using correla- tions such as the Macleod-Sugden correlation [8,9], which was extended by [10] to the form in Equation 4:

$$\sigma = \left[\sum_{i=1}^{N_c} P_i \times (\rho_L^m x_i - \rho_V^m y_i)\right]^4 \tag{4}$$

Figure 2 shows the distribution of surface-tension values in the compositional space of a three-component system, where no value is calculated in the single- phase region. Figure 2 also shows the interpolation parameter in the composi- tional space using Eq. 2 [6]. Note that a value of one is used for the single-phase region. Hence, miscibility in the relative permeabilities is only reflected in the two-phase region close to the critical point, where IFT values are close to zero.
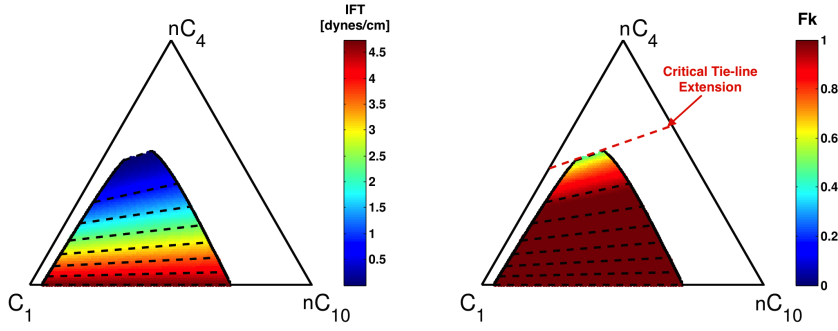
Fig. 2 *Ternary plots of the 3-component system* $(C_1 - nC_4 - nC_{10})$ *at a pressure of 100 bars and 400 K showing surface tension in dynes/cm (left) and the interpolation parameter F_k based on Equation 2 (right) using a $\sigma_0 = 1dyne/cm$ and $n = 0.2$.*

We will show one first contact miscible (FCM) example from [11] using the IFT correction presented by [6] to highlight one potential drawback of such methods. Additional cases are shown in the appendix that clarify how these methods work in different conditions. The 3-component case is one-dimensional with pure CO_2 injection at one end, and a producer at the opposite end. A controlled pressure setting is used for the wells with a pressure of 1 bar above and 1 bar below the initial condition for the injector and producer, respectively. The grid is initialized with 40% nC_4 and 60% nC_{10} at 131 bars and 344K. The grid used is made up of 1000 grid blocks ($0.1 \times 10 \times 10$ meters) with a permeability of 200 md, and a porosity of 20%. Very small time steps (0.01 days) are forced on the simulator simply to minimize the time truncation errors (max CFL number of 0.06). The simulation is run for a total of 80 days using the Peng-Robinson equation of state. The immiscible relative-permeability curves used are shown in Figure 24; the 45° diagonals shown on the right of Figure 1 are used as the miscible set.
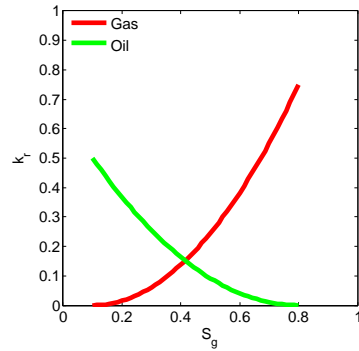

Fig. 3 *Relative permeability curves generated using the Corey correlation with $S_{gr} = 0.1$, $S_{or} = 0.2$, $k_{ro-ep} = 0.5$, $k_{rg-ep} = 0.75$ and an exponent of 2*

The pressure in the FCM displacement high enough that we no longer have a two-phase envelope in the compositional space (Figure 4). Since this phase is always identified as either single-phase gas, or single-phase oil, we only use the end-points of the relative permeability curves. No correction is applied at all in this run with the results overlapping in both cases.

The issue with the method described is the absence of any correction in the region above the critical tie-line from both physical and numerical aspects. We expect that it becomes difficult to distinguish between phases in the super-critical region; hence, using the immiscible set of relative-permeability curves (end-points) may be questionable. Numerical difficulties also arise in gridblocks near the super-critical region, for which the phase state is ambiguous and difficult to identify. The phase label can change between nonlinear iterations due to changes in both composition and pressure in addition to numerical dispersion. Changes in the phase label can lead to discontinuous jumps in the relative permeability values with consequent numerical challenges and changes in the numerical solution path. [5,12] elaborate more on such discontinuities and numerical challenges.
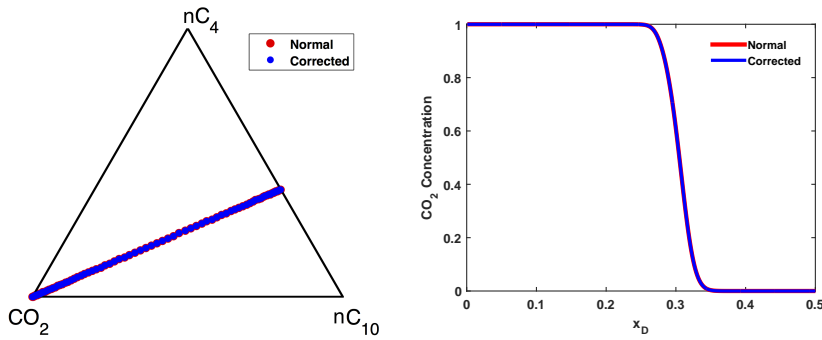

Fig. 4 *Ternary representation of the compositional path (left) and CO_2 concentration (right) for case 3 with and without corrections.*

An important observation is the jump in the relative-permeability value between the two end-points when the phase identification switches from oil to gas. A zoomed-in image of the relative-permeability values and the overall composition in the region where the phase identification flips ($x_D = 0.25 - 0.35$) is shown in Figure 5. This discontinuity highlights the necessity of incorporating compositional dependence in the single-phase region. Note that this discontinuity can also appear in two-phase displacements if the k_r curves are tightly linked to a particular phase label. This brings us to the second category of methods which aim to address this discontinuity.
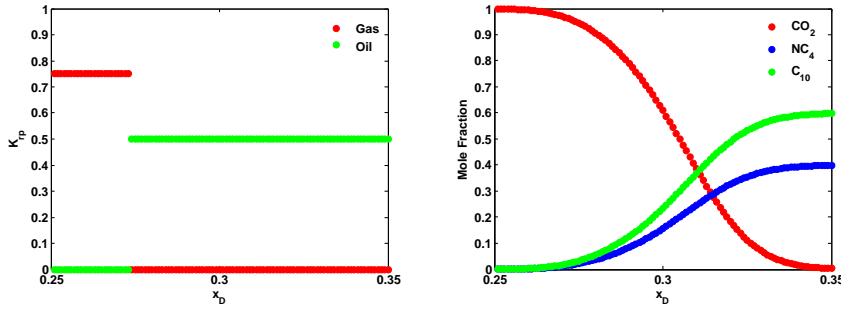
Fig. 5 *Relative permeability values showing discontinuous jump across a phase change (left) with the corresponding composition showing a continuous change (right)*

2.2 Compositional Consistency

Compositionally consistent methods aim to avoid discontinuities in the relative-permeability caused by phase labeling (e.g., oil vs. gas). The argument is that the relative-permeability relations should dependend on composition instead of depending solely on the phase-label and associated phase-saturation. These discontinuities are encountered in the critical region above the critical tie-line extension, where the phase label changes from one to the other. Figure 6 shows the relative permeabilities in the single-phase region of a 3-component system. Notice the sharp discontinuity along a line that extends above the critical point; the jump separates the single-phase region identified as oil on the right (with an end-point value of 0.5) from the single-phase gas on the left (with an end-point value of 0.8). The change of the phase label (e.g., oil vs. gas) due to small changes in composition is what we refer to as *phase flipping*.

Phase labeling in the super-critical region indicates whether the single-phase mixture is gas-like, or oil-like. Phase identification for super-critical mixtures is usually obtained using simple correlations, such as those presented by [13]. This phase-flipping discontinuity also exists using other approaches for determining the phase behavior, including the compositional space parameterization (CSP) approach [14]. The assumption in CSP is that the phase-state of a composition on the extension of a critical tie-line does not change with an increase in pressure. This ambiguity in the phase label in the super-critical region underlines the need for including compositional dependence in the relative permeability relations.
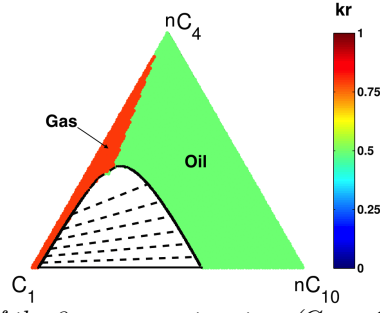
Fig. 6 *Ternary plot of the 3-component system $(C_1 - nC_4 - nC_{10})$ at a pressure of 138 bars and 411 K. Shown is the gas-oil relative permeability in the single phase region using a gas end-point of 0.8 and oil end-point of 0.5 highlighting the phase flipping region.*

The idea of compositional consistency was first introduced by [15]. [16] elaborates on the concern in three-phase situations when it becomes unclear whether a hydrocarbon phase is gas or oil. Therefore, a key requirement to ensure compositional consistency is a single hydrocarbon/water relative permeability at miscibility:

$$k_{ri} = \frac{S_i}{1 - S_w} k_{rhw}(S_w) \tag{5}$$

Here, i represents either oil or gas. A saturation-based weighting of the overall hydrocarbon-water relative-permeability (k_{rhw}) is indicative of the miscible nature of the two 'phases' where saturation is equal to concentration. The hydrocarbon-water (k_{rhw}) relative permeability curve can be obtained by interpolating between the oil-water (k_{row}) and gas-water (k_{rgw}) curves. This is done using the same interpolation-parameter idea that was used to interpolate between the immiscible-miscible limits. However, in this case the interpolation is done between the oil-gas limits (Equation 6).

$$k_{rhw}(S_w) = F_k \times k_{row}(S_w) + [1 - F_k] \times k_{rgw}(S_w) \tag{6}$$

The interpolation parameters in these methods are functions of a compositional indicator that can distinguish between the oil-like/gas-like character of the single phase. [16] proposed using the parachor-weighted molar density as a measure of composition in the following form:

$$F_k = max \left[min \left(\frac{\xi_i - \xi_{g0}}{\xi_{o0} - \xi_{g0}}, 1 \right), 0 \right] \tag{7}$$

Here ξ_i is the parachor-weighted molar density in simulation grid block i. The immiscible gas and oil limits are inputs and represented by ξ_{g0} and ξ_{o0} respectively. In this form, an F_k value of zero indicates gas, and one indicates oil. Anything in-between will be linearly interpolated between these two limits. Several authors address this approach in different ways [17–19].

An example presented by [20] for a 3-component multi-contact miscible displacement can help clarify how compositionally consistent methods work. The parameters used are similar to that of Yuan, except that only two phases are used in this example as opposed to three (Table 1). The normalized Gibbs free-energy parameter (g^* - elaborated on in Equation 8) is used as a compositional indicator instead of the parachor-weighted molar density (ξ). The reference values correspond to the maximum gas and minimum oil values from Figure 7.

Table 1 *Relative permeability parameters (Corey) and Gibbs reference points for [20] example*

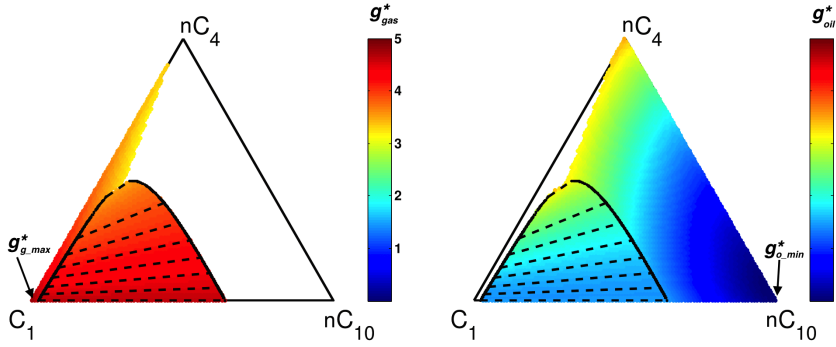| Phase	k_{rp-ep}	S_{rp}	n_p	g^*_{p0}
Oil	0.35	0.20	3.0	2.4e-6
Gas	1.00	0.15	3.0	4.81

Fig. 7 *3-component system ($C_1-nC_4-nC_{10}$) at 130.8 bars and 411K showing normalized gibbs energy of the gas phase g^*_g (left) and of the oil phase g^*_o (right).*

An initial composition of 80% nC_4 and 20% nC_{10} was used with pure C_1 injection at $x_D = 0$ with a fixed pressure of 132 bars, and production at $x_D = 1$ with a fixed pressure of 130 bars. The initial pressure and temperature are 130.8 bars and 410.95 K, respectively. The model used 1000 grid blocks of size 0.01×10×10 m with a permeability of 10 md, and porosity of 20%. Figure 8 shows the compositional path in the ternary space with the corresponding relative-permeability values for all the gridblocks in the normal (standard) case (i.e., no k_r corrections). Notice the sharp discontinuity in relative permeability as the phase label changes between oil and gas. Using a compositionally consistent model removes this discontinuity by interpolat-

ing between the two limits with changes in composition. Figure 9 shows the difference in both saturation and relative permeability distribution once the correction is used. The relative-permeability becomes a continuous function that depends on composition, and not on how the phase is identified (gas or oil).
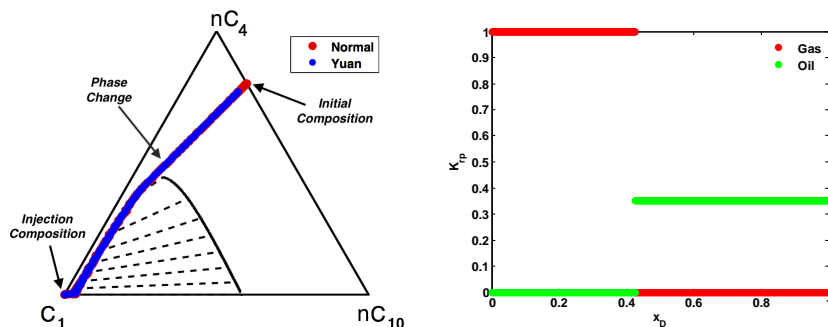

Fig. 8 *3-component system (C_1-nC_4-nC_{10}) at 130.8 bars and 410.95 K showing compositional path through critical point from Yuan's example (left) and corresponding relative permeabilities for the normal case (right).*
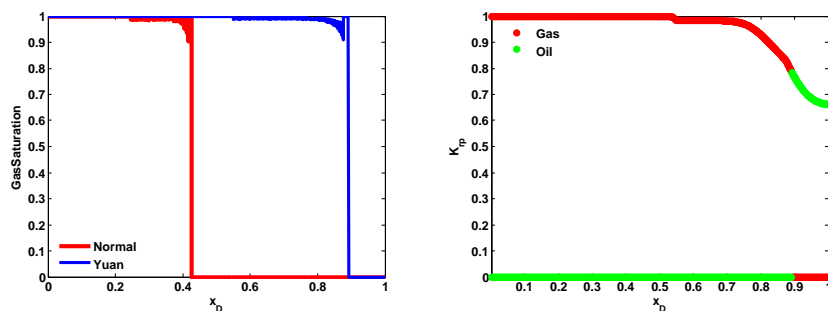

Fig. 9 *Gas saturation after 25 days with and without using Yuans correction (left) and corresponding relative permeabilties for the Yuan case (right) using max/min Gibbs free energy values as reference points.*

This approach is clearly very sensitive to the choice of the reference points; using the Gibbs free-energy from the initial composition as a reference point (reference value of 2.3 instead of $2.4e{-}6$ for the oil) leads to different saturation and relative-permeability behaviors (Figure 10).
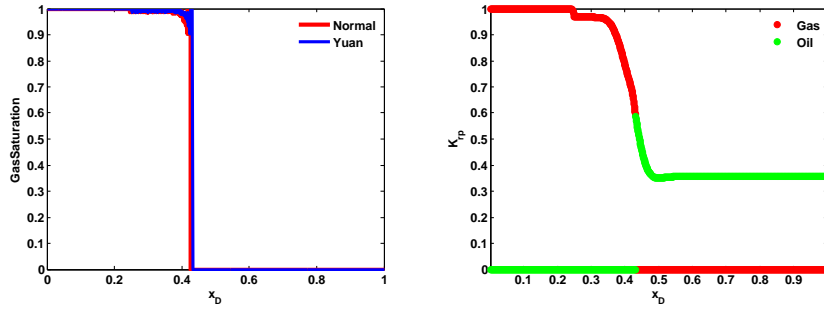
Fig. 10 *Gas saturation after 25 days with and without using Yuans correction (left) and corresponding relative permeabilties for the Yuan case (right) using initial/injection Gibbs free energy values as reference points.*

To highlight the sensitivity of the interpolation given different reference points, relative-permeability values in the compositional space are shown in Figure 11. The idea is to show how methods that interpolate between two reference points, whether using Gibbs free energy, or some other compositional indicator, can modify the relative permeability in all the compositional space including the two-phase region. Table 2 shows the reference points used for each case.

Table 2 *Reference g^* used for the different cases in Figure 11 that uses the form of Equation 7 for F_k*

Case #	g^*_{oO}	g^*_{gO}	Source of Reference Points
1	-	-	No interpolation is used
2	2.4e-6	4.81	Maximum gas/minimum oil Gibbs free energy
3	2.3	4.81	Gibbs free energy of initial/injection compositions
4	2.8	3.4	Gibbs free energies close to the critical point

Row #2 in Figure 11 shows a significant change compared to row #1 in both the single and two-phase regions. The question is whether this modification is valid. A more conservative approach might address the phase flipping region in particular without impacting the rest of the compositional space. Using reference points close to the critical region achieves just that as shown in row #4. Understanding what is physically consistent is key in order to make better use of these models. In the next section, we propose an idea that integrates both miscibility and compositional consistency.
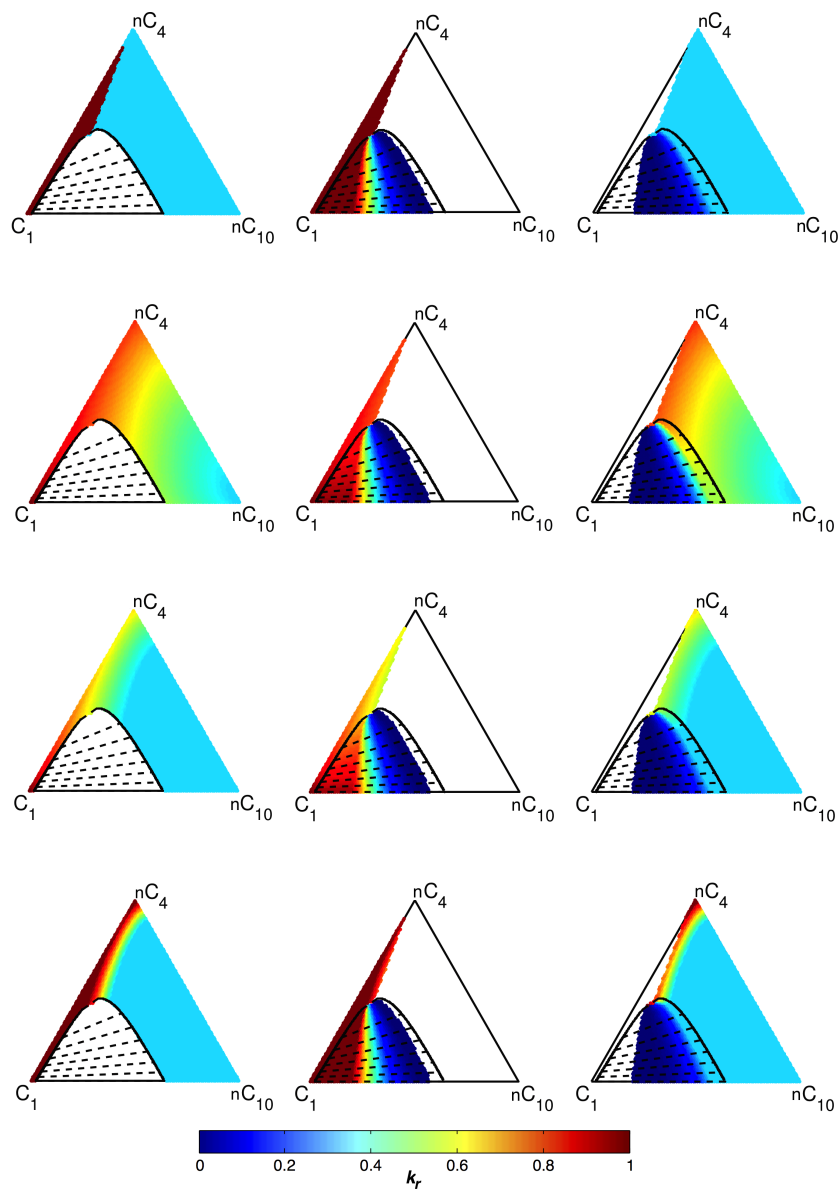
Fig. 11 *Variations of relative permeabilities in compositional space in the single phase (left), gas (middle) and oil (right) regions for the cases in Table 2 using the following interpolation methods:*

Row #1: *Standard relative permeabilities without any modifications.*
Row #2: *Yuans model with max and min values as ref. points (Fig. 9).*
Row #3*: Yuans model with init./inj. compositions as ref. points (Fig. 10)*
Row #4*: Yuans model using reference points close to critical point.*

2.3 Integrated Framework

Incorporating both objectives is not new. [15–18] have all aimed to capture miscibility and ensure compositional consistency in their relative-permeability models. The issue we deal with here is where and how the corrections are applied in a numerical flow simulation.

It appears that in more recent methods miscibility is reflected only in the two-phase region near the critical point, whereas compositional dependence is applied in all of the compositional space as shown in Figure 11. We question the validity of a linear interpolation between the oil and gas limits across all the compositional space to ensure compositional consistency. We argue that since compositional consistency becomes an issue only in the super-critical (phase flipping) region, an alternative approach is to incorporate miscibility in this super-critical region. Therefore, incorporating miscibility in both the two-phase near-miscible conditions and super-critical regions will eliminate any discontinuities in the relative permeabilities, and reflect miscible behavior in the appropriate regions of the compositional space. [15] suggests such an approach; they employ the parameter σ to represent the oil-gas IFT in the two-phase region and a pseudo-IFT for the single-phase region, where the properties of the missing phase are estimated. The following sections present the steps to implement the integrated framework that attempts to capture miscibility in all of the compositional space. Examples highlighting the impact on simulation results and performance are also presented. What is lacking in this study is experimental evidence on the exact nature of miscibility in the near-miscible and super-critical regions.

3 Numerical Implementation

We start with a list of requirements for a general relative-permeability model. The general requirements to properly capture miscibility and ensure compositional consistency are as follows:

1. The relative permeabilities should approach the expected 45° diagonals as miscibility is approached in the two-phase region close to the critical point.
2. We expect the fluid mixture to become fully miscible in all proportions in the single-phase super-critical region (i.e., above the critical tie-line extension).
3. The relative-permeability should be continuous no matter how we label the phase (oil vs. gas), and should depend on the composition.

We use the Gibbs free-energy parameter as a compositional indicator as suggested in [19]. We show how this parameter can be used to meet these requirements. The equation used to estimate the normalized Gibbs free energy [21]:

$$g_p^* = \sum_{i=1}^{N_c} x_i ln(f_{pi}), \qquad (8)$$

where x_i is the phase molar fraction, and f_{pi} is the fugacity of component i in phase p. The fugacity is obtained from the flash calculation. The normalized Gibbs free-energy (g^*) is equivalent to G/RT. The reason for using the Gibbs free-energy is that it is an intensive thermodynamic property that is continuous in the entire compositional space (Figure 7). Note that each tie-line has a unique Gibbs free-energy for each phase at fixed pressure and temperature [22].

3.1 Miscibility in the two-phase region

We can use the individual phase Gibbs free-energy as a miscibility indicator, since both are identical at the critical point (Figure 7). Taking a simple ratio in the form of Equation 9 gives an interpolation parameter that goes to zero at miscible conditions and unity at immiscible conditions.

$$F_k = 1 - \left(\frac{g_o^*}{g_g^*}\right)^n \qquad (9)$$

The Gibbs free-energy of the gas (lighter) phase is in the denominator, since it is always higher than that of the oil (heavier) phase. This is because the lighter components will have a higher fugacity than the heavier components. Since the Gibbs free-energy can have a negative value (usually encountered in the heavier phase), we impose the following constraint:

$$F_k = 1 - max\left(\frac{g_o^*}{g_g^*}, 0\right)^n \qquad (10)$$

The convenience with this approach is the ability to capture similar behavior as previous models without introducing a reference value (surface tension, or capillary number). Instead, it only requires an input exponent n, similar to the previous models, to control how fast we start to observe changes in F_k as the critical point is approached. However, due to the absence of the reference value we loose some flexibility in tuning it to match experimental behavior. Figure 12 shows a comparison between the two approaches using a reference IFT of 2 dynes/cm and exponent of 0.2 for the approach used by [6], and an exponent of 5 for the model based on Gibbs free energy. The most important feature of these models is that they capture the low F_k values as the critical point is approached.
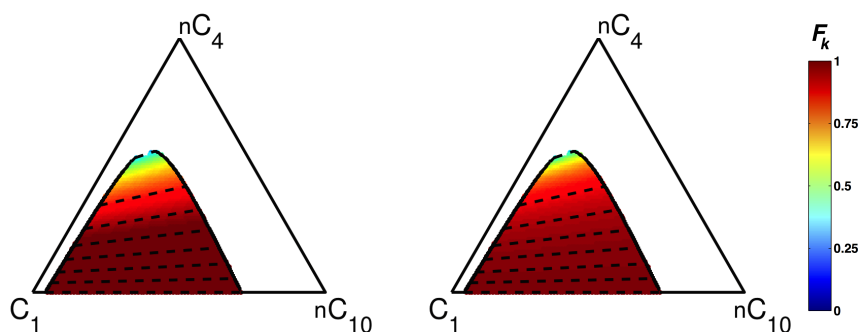
Fig. 12 *Interpolation parameter F_k using [6] IFT approach (left) and proposed approach (right).*

3.2 Miscibility in the single-phase region

The last two requirements are met by applying the miscibility correction in the region above the critical-tie-line extension. Instead of interpolating between the relative permeabilities of the two phases to ensure compositional consistency, we use the Gibbs free energy as a miscibility indicator in the super-critical region; this ensures that the relative permeability vary smoothly with composition. A reference value is needed in order to achieve this. Figure 13 shows the phase-flipping in the single phase region on the left and the Gibbs free energy on the right.
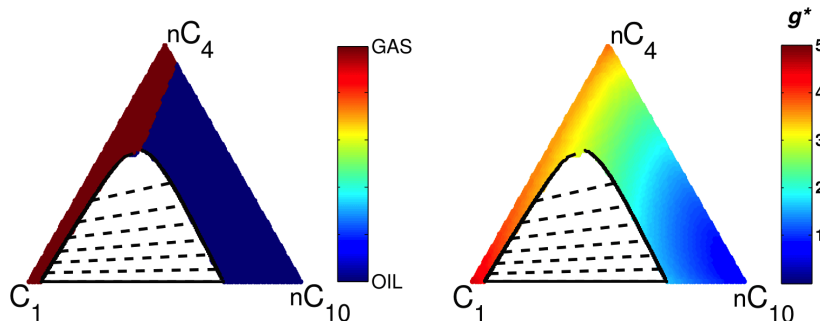

Fig. 13 *Phase IDs (left) and Gibbs free energy (right) for the three component system (C_1-nC_4-nC_{10}) at 100 bars and 450 K.*

Note how the Gibbs free-energy values along the phase flip region are very similar. This allows for a consistent change across the phase flip with a reference value that is close to the Gibbs free energy value at the critical point. Thus, we use the Gibbs free energy at the critical point as the reference point, which varies continuously as a function of pressure and temperature. This reference point is used to identify the miscible region where an F_k value of zero will be assigned to reflect full miscibility. Equation 11 can be used, which is similar to Equation 10 but with a modification to account for the fact that the gas Gibbs energy values should be higher than the reference value and the oil is expected to be lower.

$$F_k = 1 - max \left[\frac{min(g_i^*, g_0^*)}{max(g_i^*, g_0^*)}, 0 \right]^n \tag{11}$$

Here g_i^* is the normalized Gibbs energy for the single phase cell i, and g_0^* is the reference point (normalized gibbs energy at the critical point). The smaller the exponent n, the larger the area of influence is. An important difference between this approach and other compositionally consistent approaches is that this still depends on phase identification. However, the sensitivity to the phase label is reduced near miscibility and therefore avoids the complications involved with phase identification. Other methods interpolate between reference states without any dependence on the phase label in all of the compositional space. Figure 14 illustrates the effect of this approach assuming relative permeability end-points of 0.8 and 0.5 for the gas and oil respectively and a reference Gibbs free energy of 3.04. Notice the correction focused near the critical point and above it near the phase flip region.

The main idea here is to present an integrated approach where incorporating miscibility in all of the compositional space ensures compositional consistency. However, this ultimately needs to be validated with experimental evidence. The exact natures of the transitions need to be physically justified. We believe there is an opportunity to build on such models. Many of the changes across phase boundaries and between sub- and super-critical regions can be related to the CSP framework, and the continuity of the parameterized compositional space presented by [23]. Also, the use of Gibbs free energy might be further exploited as it is intimately related to thermodynamic stability. [22] shows how CSP yields the global minimum of Gibbs energy, where such a framework can help in identifying better ways of reflecting miscibility in the super-critical region. The next section will present the impact of such methods on simulation results and performance.
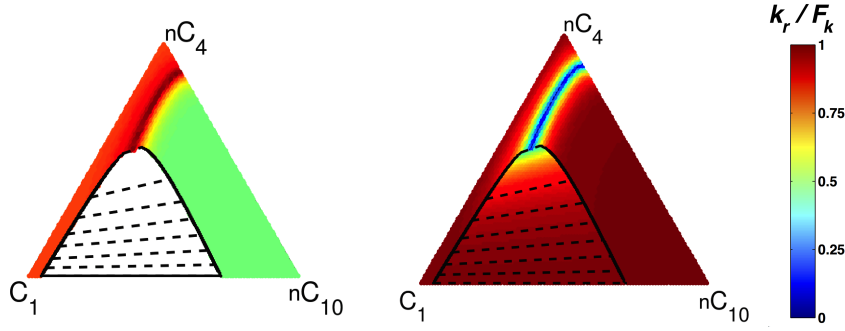
Fig. 14 k_{ro} and k_{rg} in the single phase region (left) with corresponding F_k interpolation parameter in all the compositional space (right) using a $g_0^* = 3.04$ and $n = 20$ for the single phase region (Eq. 11) and $n = 5$ for the two phase region (Eq. 10).

4 Results

4.1 2D - 3-component example

The system we consider is made up of $C_1 - nC_4 - nC_{10}$, and is run on layer 30 of the SPE10 model shown in Figure 15 [24]. One injector well located in the top-left corner (1×1) is injecting pure C_1 at a fixed BHP of 140 bars. The single producer is placed in the opposite corner of the grid (60×220) producing at a fixed BHP of 80 bars. The initial condition of the system is made up of 5% C_1, 15% nC_4 and 80% nC_{10} at 138 bars and 411 K. The relative permeability curves used in this model are shown in Figure 16. This case is based on the condensing gas drive presented by [25].
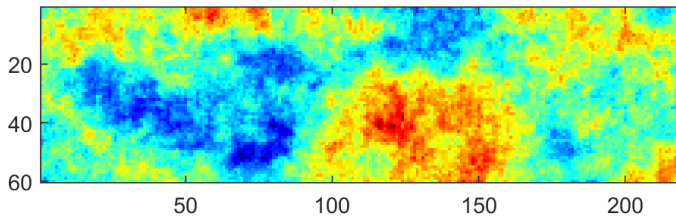

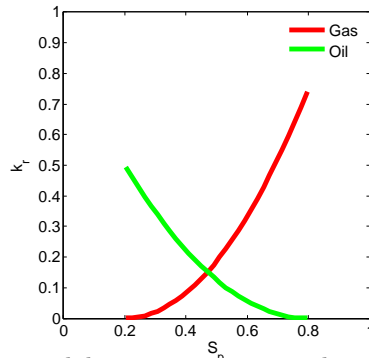**Fig. 15** $Log(k_x)$ map of 30th layer of SPE10 - block size: $3.05 \times 6.1 \times 0.61 m$

Fig. 16 *Relative permeability curves generated using the Corey correlation with residual saturations of 0.2, exponents of 2, gas and oil end-points of 0.75 and 0.5 respectively.*

In this example, we look at the differences in composition/saturation distribution maps, breakthrough times and rates, as well as nonlinear performance. Maps of the interpolation parameter F_k will help highlight the difference in where the corrections are applied and at what magnitude. This simulation was run for 8000 days with a maximum time step of 20 days using the Peng-Robinson EOS. The different cases we consider are the following:

1. Normal simulation run without any modification to the relative permeability curves [**NORMAL**]
2. Simulation run with correction in the two phase region only using IFT as an indicator [6] with a reference IFT value of 1 dyne/cm and exponent of 0.2 (Equation 2) [**IFT**]
3. Simulation run with correction in the two phase region only using Gibbs free energy as an indicator with an exponent of 5 (Equation 10) [**GIBBS**]
4. Simulation run with correction in the entire compositional space using Gibbs free energy as an indicator with an exponent of 5 for the two phase region (Equation 10) and reference Gibbs value of 3.17 and exponent of 20 in the single phase region (Equation 11) [**GIBBS-ALL**]

The first clear advantage of using any form of correction is the significant improvement in nonlinear convergence (Figure 17). This improvement translates to a significant improvement in simulation running time. The differences between the IFT and GIBBS methods are minor. Figure 18 shows the difference in the C_1 concentration distribution. The cases with correction exhibit a slightly more diffused C_1 front. The gas rate at the producer in Figure **??** shows little difference in the gas breakthrough time with slightly higher production rates for the correct. Other cases show
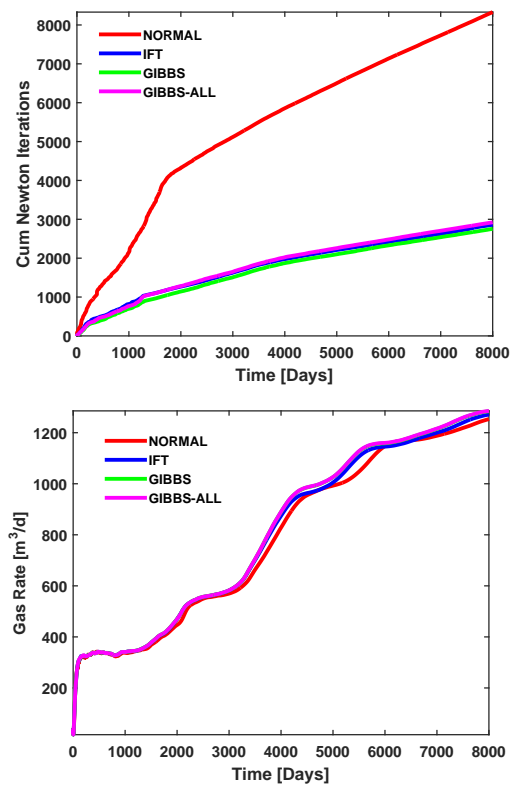
Fig. 17 *Cumulative Newton iterations showing significant improvement in the cases that incorporate compositional dependence (top). Gas production rate showing no significant different in production rates with only a slightly higher rate in the corrected cases caused by a more diffused front (bottom).*
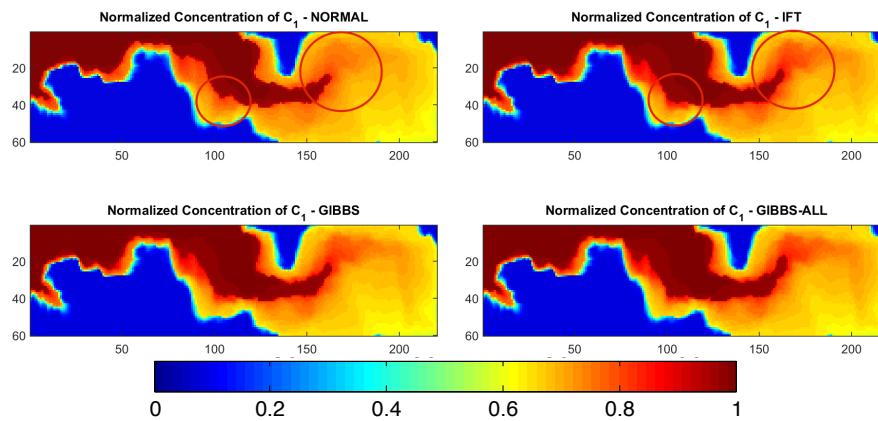

Fig. 18 C_1 *normalized concentration for the different cases showing a slightly more diffused C_1 concentration in the cases with correction.*

Figure 19 shows the interpolation parameter F_k map. The IFT and GIBBS case apply the correction in the two-phase region only where the GIBBS case covers a larger area since no reference value is used that enforces a cut-off. The discontinuity between the single and two-phase regions in these two cases is eliminated in the GIBBS-ALL case that makes use of the single-phase region correction. Notice how the highest correction occurs in the trailing edge indicating a condensing gas drive mechanism as outlined by [25] for 3-component systems.
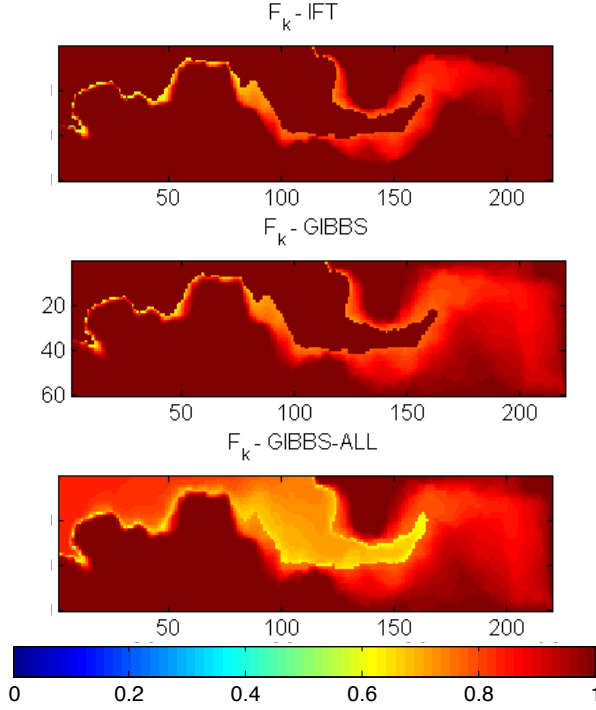

Fig. 19 F_k map showing the highest correction at the trailing edge. GIBBS-ALL case shows the correction being applied to the single phase region as well.

Figure 20 shows the compositional path on a ternary diagram for the GIBBS and GIBBS-ALL case (note the phase envelope shown is for a pressure of 139 bars and temperature of 411 K). The main point here is to show the compositional path, and the corresponding interpolation parameter F_k, with the same trend of decreasing value towards the critical point. However, the GIBBS case applies no correction to the points that lie outside the two-phase region above the critical point (near the injection condition between C_1 and nC_4). This is reflected onto the relative permeability values with a sudden change between the single and two-phase regions (Figure 21).
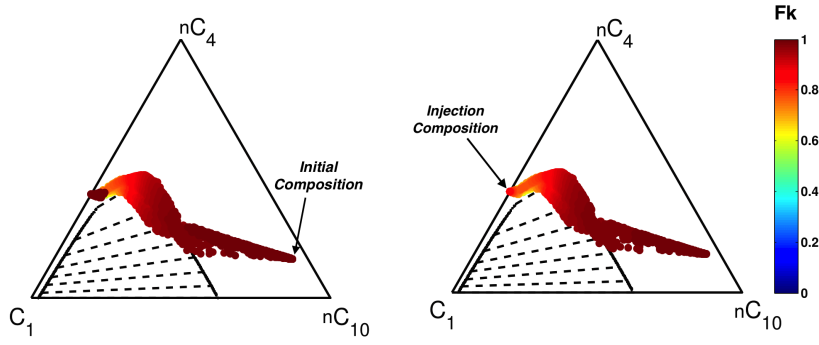
Fig. 20 *Compositional path of GIBBS (left), and GIBBS-ALL (right) cases showing F_k parameter values. GIBBS-ALL case applies to corrections to grid blocks close to the critical point just outside the two-phase envelope.*
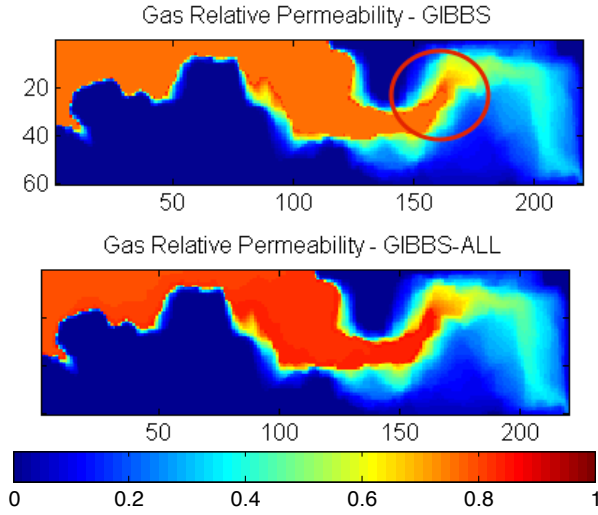

Fig. 21 *Gas relative permeability for the GIBBS (top) and GIBBS-ALL (bottom) cases showing a discontinuous jump in the relative permeability values for the GIBBS case between the single and two-phase regions.*

This example shows the significant improvement in nonlinear performance that can be attained when using relative permeability curves that are closer to the 45° diagonals in the near-miscible region. It is important to note that the cases end up with different CFL numbers due to different phase velocities and time truncation-errors; the max CFL averaged in all the time steps for each case in the order they were listed are: 150, 193, 196 and 197. The improvement in nonlinear iterations is achieved despite the higher CFL numbers.

The difference between the choice of two-phase correction is minor. Both are obviously affected by the parameters used, where the IFT approach has two parameters and the Gibbs has only one. In this case using the Gibbs free energy as an indicator took less Newton iterations. Whether the single-phase correction is physically accurate can still be questioned, and needs further investigation and validation. However, it does result in more consistent relative permeability values by eliminating the small jump between the single and two-phase regions (Figure 21). The next section will discuss the sensitivity of the different models to different realizations.

4.2 Sensitivity

In order to assess the sensitivity of the different models, we simply ran the same case in section 4.1 on all 85 layers of SPE10. Figure 22 shows the total number of Newton iterations and corresponding simulation run time for all the layers. The results clearly show a significant improvement from the NORMAL case for all corrections used. We only observe slight differences between the different methods as shown in Table 3.
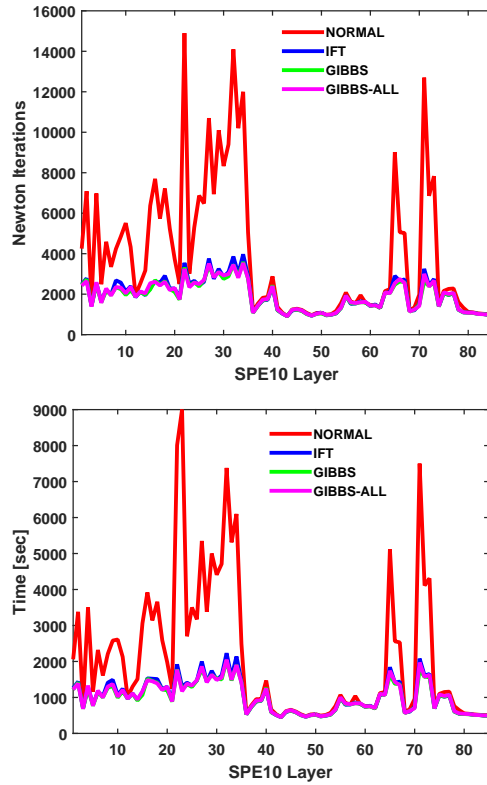

Fig. 22 *Cumulative Newton iterations (top) and total run time (bottom) for each SPE10 layer.*

Table 3 *Average Newton iterations and run time for the 3-component model on all SPE10 layers*

Case	Average Newton iterations	Average run time [sec]
NORMAL	3882	2083
IFT	1969	1043
GIBBS	1904	1006
GIBBS-ALL	1927	1020

There is a clear shift in performance of the NORMAL case from layers 1-34 and 35-65. This is caused by the different nature of permeability distributions in these layers, which indicates that the NORMAL case faces fewer diffculties in the channeled layers (35-65). The reason for this could be less miscibility development in these systems. In addition to different realizations, sensitivty was run on different exponents for equations 10 and 11. The results are shown in Figure 23.
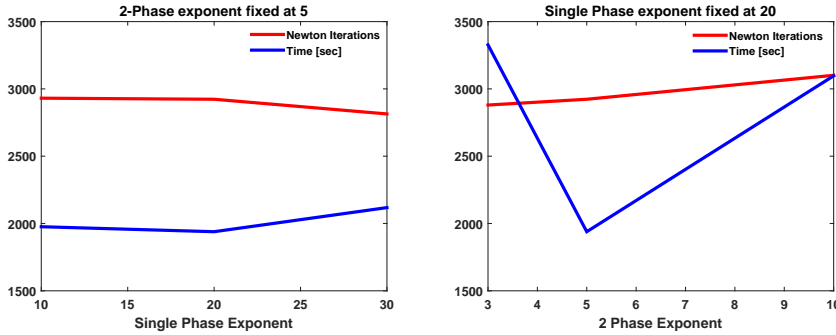

Fig. 23 *Cumulative Newton iterations and total run time for different single-phase exponents (left) and two-phase exponents (right) for the GIBBS-ALL equations shown in equations 10 and 11.*

In general we see the same performance in terms of non-linear iterations. As the exponent values increases, the area of influence around the supercritical region should decrease (Figure 12 and 14), which means less correction. We see a slight decrease in newton iterations with a slight increase in run time as the single-phase exponent increases. The non-linear iterations slightly increase with larger two-phase exponents with strange behavior for the run time. This requires further investigation.

5 Conclusions

Accounting for compositional dependence in the relative-permeability relations is important for accurate and robust compositional flow simulation of gas-injection processes. Existing methods focus on miscibility within the two-phase envelope; this raises the question of the validity of treating all cells outside the phase envelope in the same manner. We described possible approaches for incorporating miscibility in regions inside and outside the two-phase envelope; we use the normalized Gibbs free-energy parameter. The motivation is that incorporating miscibility in all of the compositional space is expected to be more representative of the physics, while also resolving the discontinuities in the relative permeabilities across the phase-flipping region. We have shown that the type of linear interpolation in compositionally consistent methods can have significant effects on the entire compositional space with sensitivity on the chosen reference points. A more solid physical basis of how the relative permeabilities vary with composition is needed to ultimately justify the k_r treatments used here.

6 Nomenclature

k_{rp}^{Cor}	corrected relative permeability of phase p
k_{rp}^{Imm}	immiscible relative permeability of phase p
k_{rp}^{Mis}	miscible relative permeability of phase p
k_{rp-ep}	endpoint relative permeability of phase p
F_k	interpolation parameter
σ	surface tension [dynes/cm]
σ_0	reference surface tension [dynes/cm]
n	exponent
N_{cap}	capillary number
u	superficial velocity [m/s]
μ	viscosity [cp]
α	rock dependent constant from [7]
N_c	number of components
P_i	parachor of component i - empirical constant $[(dyne/cm)^{1/4}(m^3/mol)]$
x_i	liquid molar fraction of component i
y_i	vapor molar fraction of component i
ρ_L^m	liquid molar density [gram-Mole/cc]
ρ_V^m	vapor molar density [gram-Mole/cc]
N_{cap}	capillary number
S_i	saturation of phase i
ξ_i	parachor weighted molar density of cell i $[(dyne/cm)^{1/4}]$
ξ_{p0}	reference parachor weighted molar density of phase p $[(dyne/cm)^{1/4}]$
f_{pi}	fugacity of component i in phase p [bars]
g_p^*	normalized Gibbs free energy of phase p
g_i^*	normalized Gibbs free energy of cell i
g_0^*	reference normalized Gibbs free energy
x_D	dimensionless distance

References

1. L.W. Lake, (1989)
2. F.M. Orr, *Theory of gas injection processes* (Tie-Line Publications Copenhagen, 2007)
3. S.M.P. Blom, *Relative permeability to near-miscible fluids* (TU Delft, Delft University of Technology, 1999)
4. Y.M. Al-Wahaibi, C.a. Grattoni, a.H. Muggeridge, Journal of Petroleum Science and Engineering **53**, 239 (2006). DOI 10.1016/j.petrol.2006.06.005
5. A.N. Alzayer, Relative permeability of near-miscible fluids in compositional simulators. Master's thesis, Stanford University (2015)
6. K. Coats, Society of Petroleum Engineers Journal **20**(October), 363 (1980). DOI 10.2118/8284-PA
7. O.i. Fevang, C.H. Whitson, SPE Reservoir Engineering (November) (1996)
8. D. Macleod, Trans. Faraday Soc. **19**(July), 38 (1923)
9. S. Sugden, Journal of the Chemical Society **125**, 32 (1924)
10. C.F. Weinaug, D.L. Katz, Industrial & Engineering Chemistry **35**, 239 (1943). DOI 10.1021/ie50398a028. URL http://pubs.acs.org/doi/abs/10.1021/ie50398a028
11. R. Metcalfe, L. Yarborough, Soc. Pet. Eng. J **19**(8), 242 (1979)
12. H. Cao, R. Zaydullin, E. Obi, et al., in *SPE Reservoir Simulation Conference* (Society of Petroleum Engineers, 2017)
13. R. Gosset, G. Heyen, B. Kalitventzeff, Fluid Phase Equilibria **25**(01), 51 (1986)
14. D.V. Voskov, H.A. Tchelepi, SPE Journal **14**(03), 441 (2009)
15. D. Tang, A. Zick, in *SPE Symposium on Reservoir Simulation* (1993)
16. G. Jerauld, SPE Reservoir Engineering **12**(November) (1997). DOI 10.2118/36178-PA
17. F. Fayers, A. Foakes, C. Lin, D. Puckett, in *SPE/DOE Improved Oil Recovery Symposium* (Society of Petroleum Engineers, 2000)
18. M.J. Blunt, SPE Journal **5**(December), 435 (2000). DOI 10.2118/67950-PA
19. C. Yuan, G. Pope, Spe J. **17**, 1221 (2012). DOI 10.2118/142093-PA
20. C. Yuan, A new relative permeability model for compositional simulation of two and three phase flow. Ph.D. thesis, University of Texas (2010)
21. C.H. Whitson, M.R. Brulé, *Phase behavior* (Richardson, Tex.: Henry L. Doherty Memorial Fund of AIME, Society of Petroleum Engineers, 2000)
22. A. Iranshahr, D.V. Voskov, H.a. Tchelepi, Fluid Phase Equilibria **321**, 49 (2012). DOI 10.1016/j.fluid.2012.02.001
23. A. Iranshahr, D. Voskov, H.A. Tchelepi, SPE Journal **18**(6) (2013)
24. M. Christie, M. Blunt, SPE Reservoir Evaluation & Engineering **4**(August), 308 (2001). DOI 10.2118/72469-PA
25. A. Zick, in *SPE annual technical conference and exhibition* (Society of Petroleum Engineers, 1986)
26. F. Orr Jr, R. Johns, B. Dindoruk, SPE reservoir engineering **8**(02), 135 (1993)

7 Appendix

This section includes additional 1D 3 component cases to highlight how models that focus on reflecting miscibility only work, as well a 2D 4 component case to compare the different models discussed in this paper.

7.1 1D - 3-component examples

Three examples from [11] are replicated using the IFT correction presented by [6]. The 3-component cases are one-dimensional with pure CO_2 injection at one end, and a producer at the opposite end. A controlled pressure setting is used for the wells with a pressure of 1 bar above and 1 bar below the initial condition for the injector and producer, respectively. The reason for this is to ensure that the phase envelope shown on the ternary diagram is representative throughout the simulation, and therefore captures the 'true' compositional path. Table 4 shows the conditions for each case. The grid used is made up of 1000 grid blocks (0.1×10×10 meters) with a permeability of 200 md, and a porosity of 20%. Very small time steps are taken to minimize the time truncation errors (max of 0.01 days that yield a max CFL number of 0.06). The simulation is run for a total of 80 days using the Peng-Robinson equation of state. The immiscible relative-permeability curves used are shown in Figure 24; the 45° diagonals shown on the right of Figure 1 are used as the miscible set.

Table 4 *Initial conditions and compositions of [11] system 1 properties*

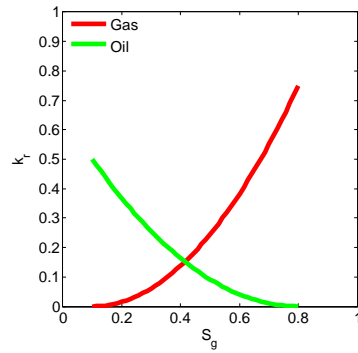| Case	Condition	CO_2	nC_4	nC_{10}	Pressure [bars]	Temperature [K]
1	Immiscible				103	
2	MCM	0	40	60	117	344
3	FCM				131	

Fig. 24 *Relative permeability curves generated using the Corey correlation with $S_{gr} = 0.1$, $S_{or} = 0.2$, $k_{ro-ep} = 0.5$, $k_{rg-ep} = 0.75$ and an exponent of 2*

Case #1 represents an immiscible displacement, since both the injection and initial conditions lie below the critical-tie-line extension. We expect very small changes to the immiscible k_r curves in this case. The compositional path is shown in figure 25, where each point represents a gridblock composition at the end of the simulation. The figure on the right shows the value of the interpolation parameter, F_k, for all the gridblocks in the compositional space with lower values near the critical point as expected. The slight difference in the simulation results is clearer for the CO_2 concentration front (Figure 26). The corresponding correction parameter (F_k) at the end of the simulation is also shown with a minimum value around 0.7 indicating a more immiscible-like displacement.
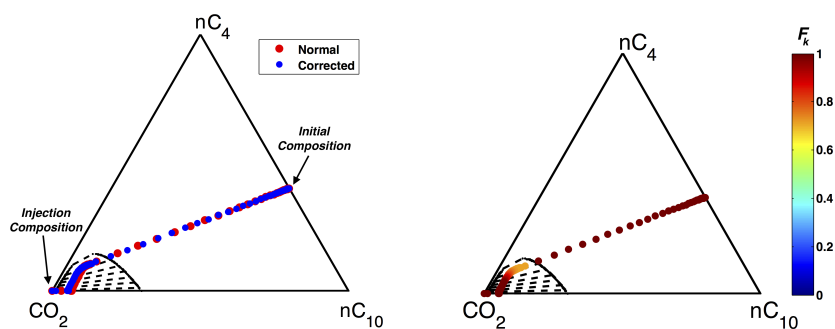

Fig. 25 *Ternary representation of the displacement in case 1 showing the compositional path (left) and the interpolation parameter F_k values for the corrected case (right)*
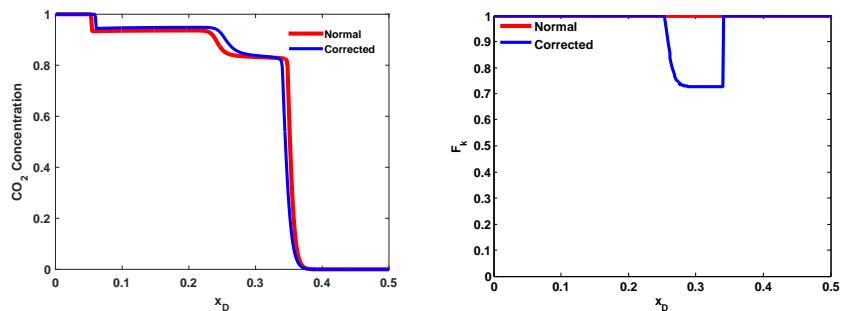

Fig. 26 *CO_2 concentration distribution at the end of the simulation with and without a correction (left) and the corresponding interpolation paramter F_k values (right).*

Case #2 is a multi-contact miscible (MCM) displacement, since the initial composition is on one side of the critical-tie-line extension with the injection composition on the other; the process involves a vaporizing gas drive mechanism. We expect to see a larger impact of the correction in this MCM displacement compared with the immiscible displacement of Case #1. The compositional path enters the two-phase envelope near the critical point and follows the dew-point line down to the injection composition (Figure 27). Figure 28 shows the CO_2 concentration front for both cases; the two plots overlay each other even though F_k is 0.3 at the miscible front. The MCM displacements show smaller changes with the 'correction' than the immiscible case. The small changes in the overall behavior can be attributed to the very small two-phase region that is encountered in such displacements.
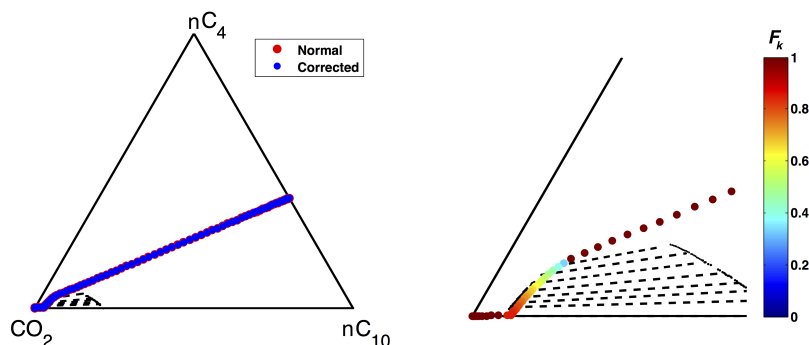

Fig. 27 *Ternary representation of the displacement in case 2 showing the compositional path (left) and the interpolation parameter F_k values for the corrected case (right)*
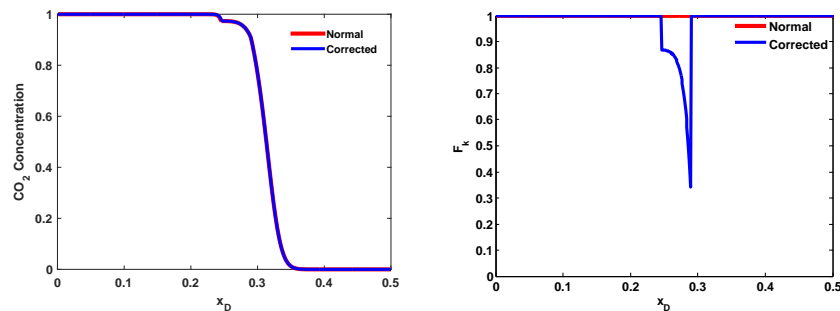

Fig. 28 *CO_2 concentration distribution at the end of the simulation with and without a correction (left) and the corresponding interpolation paramter F_k values (right).*

7.2 2D - 4-component example

The 4-component system we consider, obtained from [26], is made up of $CO_2 - C_1 - nC_4 - nC_{10}$. The case is run on the upscaled layer 15 of the SPE10 model shown in Figure 29. One injector well located in the top-left corner (1×1) is injecting pure CO_2 at a fixed BHP of 140 bars. The single producer is placed in the opposite corner of the grid (30×110) producing at a fixed BHP of 80 bars. The initial condition of the system is made up of 10% C_1, 20% nC_4 and 70% nC_{10} at 110 bars and 344 K. The relative permeability curves used in this model is the same one shown in Figure 16.
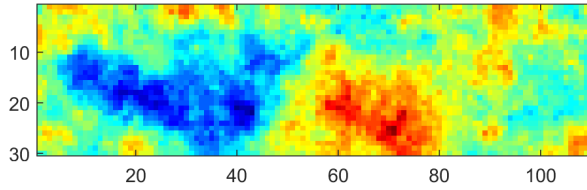

Fig. 29 *Log(k_x) map of upscaled 15th layer of SPE10 - block size: 12.2 × 6.1 × 1.2m*

We use the same cases with the same parameters in section 4.1 except for the reference Gibbs free energy that is 3.12 for the GIBBS-ALL case. A limitation in our implementation is our use of a single reference Gibbs free energy for the whole simulation run. This value should change with pressure and temperature, and in the 4-component case should capture the value of the closest critical point along the locus of critical points.

Figure 30 shows the gas and oil Gibbs free energy in the two-phase region showing the same trend observed in the 3-component systems. The Gibbs free energy of the gas is always higher than the oil in the two-phase region and decreases as the critical locus is approached. The Gibbs free energy of the oil increases as the critical locus is approached. We also show the ratio of the two approaching one around the critical locus that confirms that the behavior seen in 3-component systems is applicable to multi-component systems. The reference value of 3.12 used in this case is the maximum oil/minimum gas Gibbs free energy in the two-phase region.
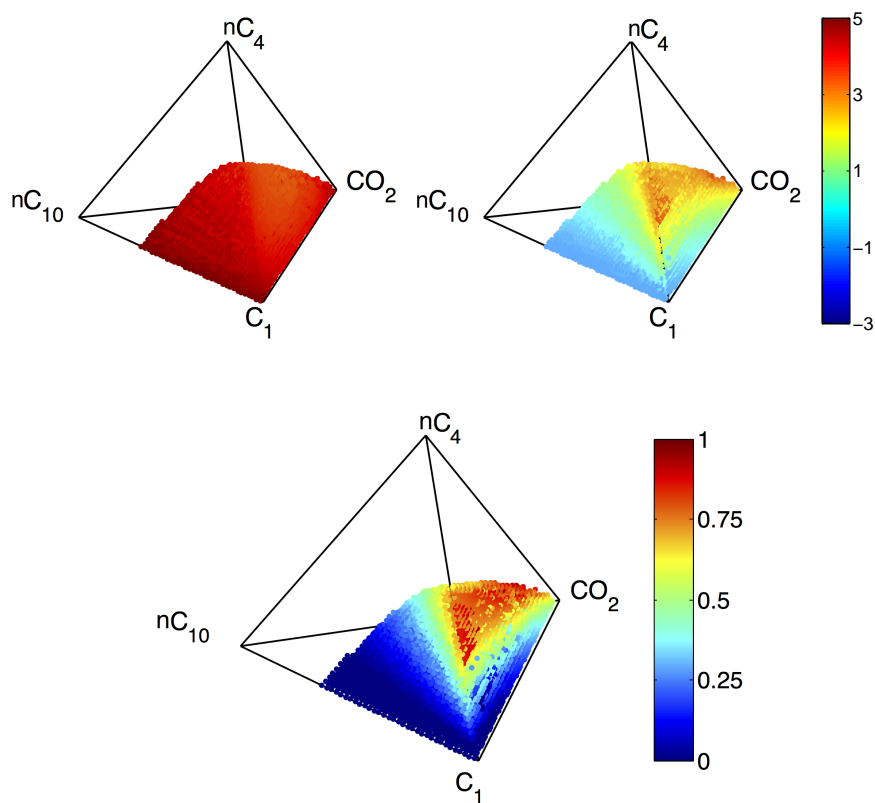
Fig. 30 *Gibbs free energy of gas (top-left) and oil (top-right) and the ratio of oil to gas (bottom) in the two phase region of the quaternary system at a pressure of 110 bars and 344 K*
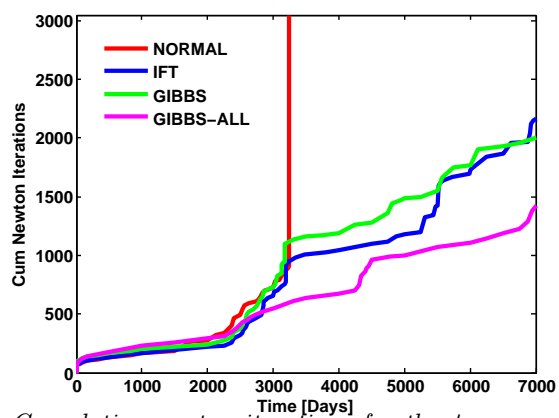

Fig. 31 *Cumulative newton iterations for the 4-component example*

The case was run for a total time of 7000 days with a maximum time step of 500 days, this resulted in a max average CFL number of 40 for the IFT and GIBBS cases, and 60 for the GIBBS-ALL case. The normal case in this example is unable to complete the simulation run due to time steps cutting to very small values. Figure 31 shows the cumulative newton iterations for each case with the normal case facing difficulties with convergence shortly after two-phase flow develops. A more in depth analysis of the nonlinear performance is required to fully understand the reasons for this difficulty. Any correction applied to the relative permeability in the near-miscible region significantly improves non-linear convergence.

Figure 32 shows the gas saturation and corresponding F_k maps. We see that not much correction is taking place in this example showing only a small region in the IFT case that has a surface tension less than 1 dyne/cm. Again, the GIBBS applies a very small correction on a larger area of the two-phase region with not much effect on the simulation results as evident in the gas production rates in Figure 33. The GIBBS-ALL case applies some correction in the single-phase region that is close to the critical locus near the injection composition (CO_2) shown on the quaternary representation in Figure 33. We observe the same behavior of the previous 3-component cases; a significant improvement in the convergence rate when applying any correction with changes in gas breakthrough times.
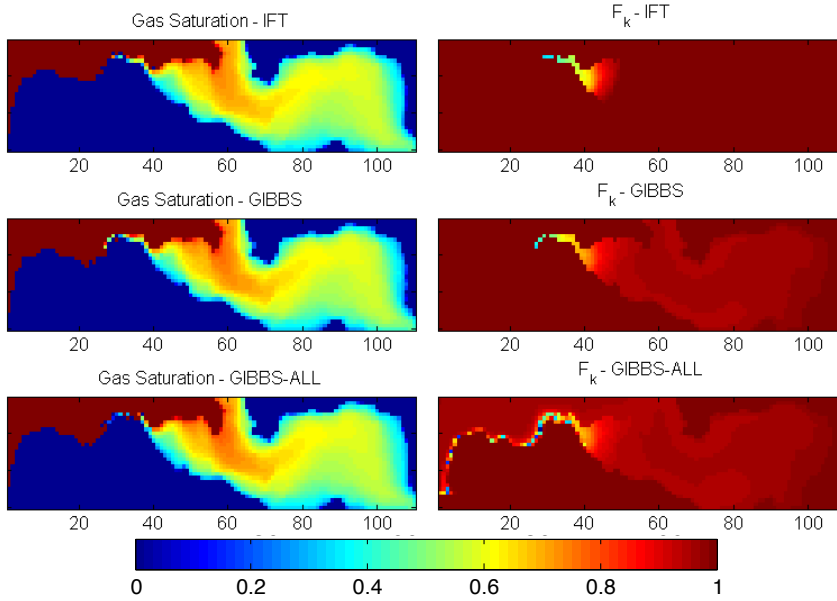

Fig. 32 *Gas saturation distribution at the end of the simulation after 7,000 days for the different cases with the corresponding F_k map*
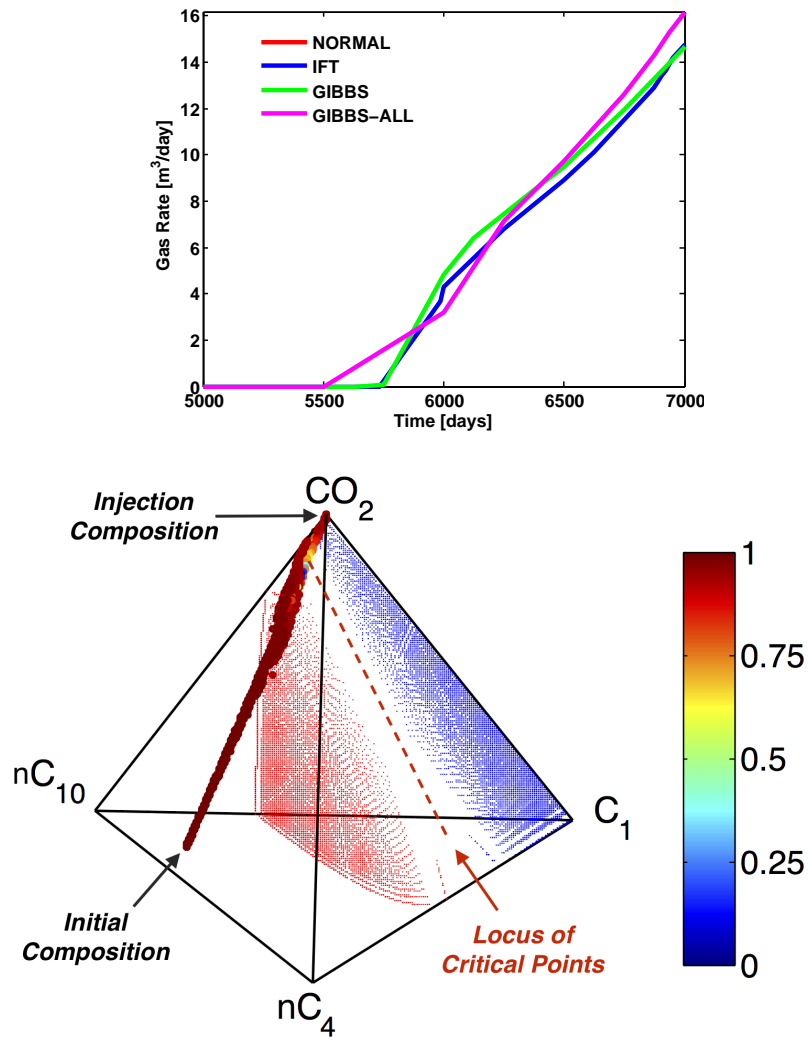
Fig. 33 *Gas production rates (top) and quaternary representation of the compositional path for the GIBBS-ALL case showing F_k values with a phase envelope constructed at a pressure of 110 bars and 344 K (bottom)*